Error Signal Generator for Ultrastable Voltage Source

semester project at

Trapped Ion Quantum Information group

Swiss Federal Institute of Technology Zurich

Supervisors:

Francesco Lancellotti
Prof. Dr. Jonathan Home

Student:

Giorgio Fabris

10 November 2021

Abstract

Magnetic field is a fundamental resource for trapped ions quantum information. However the sensitivity of qubits transitions to magnetic field fluctuations is a major source of decoherence. It is then vital for the current used to produce the field to be extremely stable. Here we completed the construction of an error signal generator which can be used in the feedback circuit for stabilizing such a current. Specifically, the casing has been built and a temperature stabilizer has been included. The device was then characterized and compared to the system currently in use. Possible improvements were also suggested and the control software has been improved too.

Contents

1 Introduction

In trapped ions quantum information, information is encoded in the ion electronic states energy levels. States with same good quantum numbers besides the orientation of the total angular momentum (m) will be degenerate, making it impossible to associate two distinguishable states as qubits states $|0\rangle$ and $|1\rangle$, which is required in quantum information processing.
In order to lift this degeneracy, Zeeman effect is exploited and so a magnetic field is applied to the trapped ions. In this way, a splitting of the levels proportional to m and to the magnitude of the magnetic field will occur. This last proportionality relation is of great importance, as it means that fluctuations of the magnetic field will result in fluctuations of the qubit resonance frequency. Hence, the qubit will be dephased and information will be lost.
There exist transitions which are, at first order, field independent, such as $|F = 2, M_F = 0\rangle \longleftrightarrow |F = 1, M_F = 1\rangle$ in beryllium. However, qubit transition is not the only one involved in experiments. For state preparation and readout, other transitions are used, hence stability of the magnetic field remains important.

In the case of study, the magnetic field is produced by a current flowing through a pair of Helmholtz coils and therefore, a stable current is required in order to have a stable magnetic field [3]. The idea is then to sense this current, read it in the error signal generator, subtract a reference voltage and generate the error which will be used by the power supply itself to modify its output accordingly.

This project focuses on the error generation part. It is important to state that the stabilization of the magnetic field is only one of the many applications this device could be used for, as it could be helpful in any situation in which an error signal is needed, as for feedback loops stabilizing either a current or a voltage source.

2 Hardware

2.1 Design and PCB

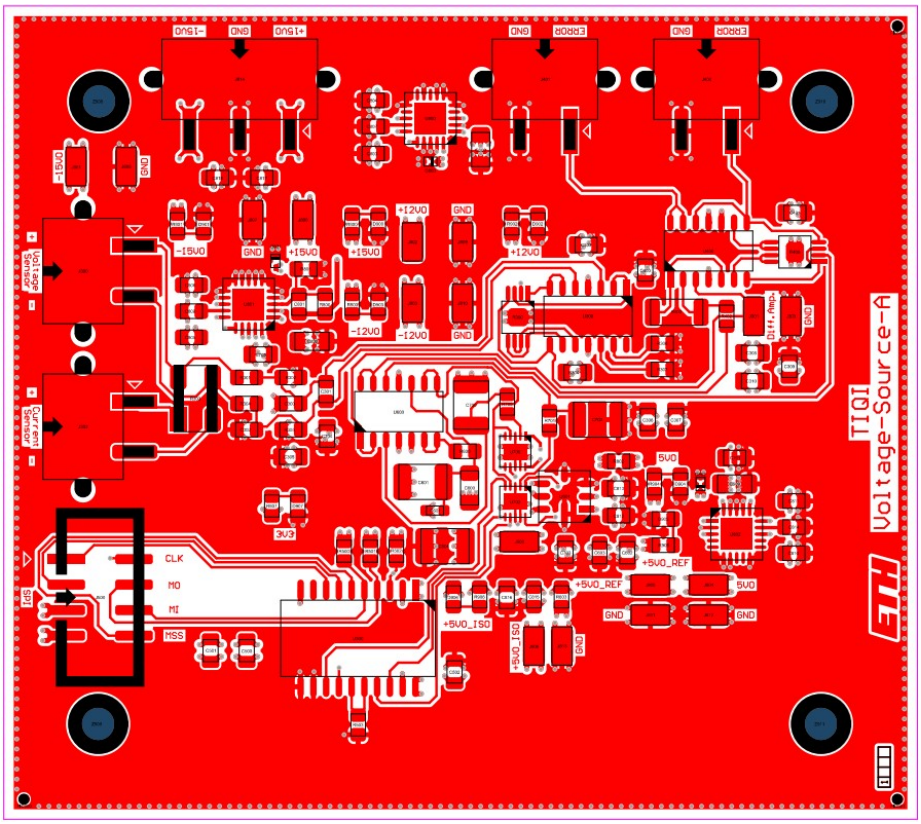

Figure 1: Top layer of PCB layout. For the schematics see Appendix A. (*From* [2])

The PCB takes as inputs either a sensed current or a sensed voltage, depending on the application. In the case of current the input is converted through a system of resistors and a differential amplifier (U300C in Appendix A) into $V_{diff} = 4.32I_s$ (not 5 as given in [1]). In the case of voltage, it is converted, through the same system, into $V_{diff} = \frac{V_s}{2}$.
V_{diff} is then amplified and a reference, which is generated by a coarse-fine pair of identical 16-bit DACs (U700 and U702), whose maximum output value is 1.9898V [1], is subtracted to it. The PCB is powered by a power supply at +15V, 0V and -15V . These voltages are filtered, stabilized and converted by some voltage regulators (U800, U801 and U802). In particular the +15V input

is converted into +12V for the supply of the operational amplifiers and into +5V for the DACs (for generating their reference voltage. See Voltage Reference in Appendix A) and the SPI isolator (U500). The -15V input is converted into -12V for the operational amplifiers. The final output of the system will be:

$$V_{ERR} = 200V_{DAC_{coarse}} + V_{DAC_{fine}} - 202V_{diff}$$

This output will be inserted in the feedback loop of the control system. Another output, equal to the previous one, is used as monitor.
In order to set the DACs voltages an SPI communication between them and a raspberry pi is used, even though no information is received from the DACs. The software used to control them will be discussed in section 3.

2.2 Temperature controller

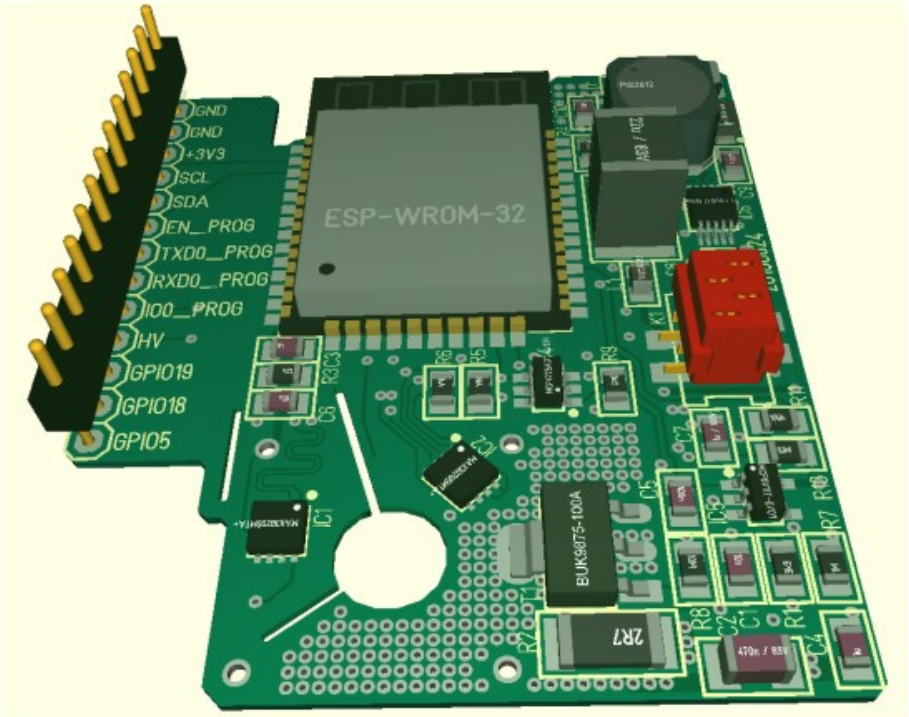

Figure 2: Temperature controller layout. (*From* [1])

The components of the PCB vary their behaviour depending on temperature (as shown in section 4), hence fluctuations in temperature will result in fluctuations of V_{ERR}. Given that stability is an essential requirement of the device, this

problem has to be addressed. A temperature controller was therefore included. In Figure 2 its layout is shown. IC1 and IC2 next to the hole at bottom left are the temperature sensors. Based on how much the sensed temperature differs from the set point a current will flow through the 2R7 resistor, which will dissipate power. This resistor is placed near the hole, where a metal screw has to be placed. The screw will then warm up and diffuse heat.

The controller is programmed such that it sets its reference automatically, based on the conditions of the environment it is placed in. In particular, it will keep temperature above the ambient one. When the button at top right (not visible in Figure 2) is pressed for more than five second, the device will forget its previous set point and start again in finding the new one. This stabilization process requires a few hours. If temperature goes above the set point, the controller will increase it accordingly, even though the process will be slow.

For communication, pins on the left are available, as well as WIFI and Bluetooth modules (ESP-WROM-32 component). However, being the controller programmed to work automatically, there is no actual need to connect to the device.
It is also possible to visualize how temperature changes in time on Grafana. However this feature was not exploited.

More information on the temperature controller can be found here
https://github.com/tempstabilizer2018group/tempstabilizer2018.

2.3 Case

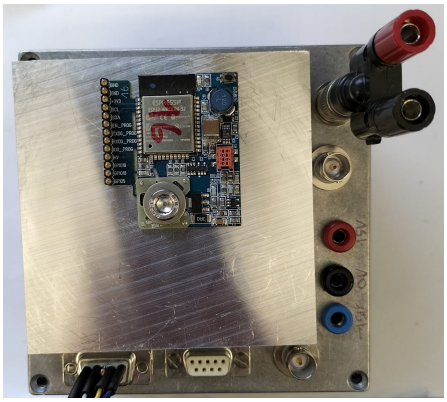

Figure 3: Top view of the case

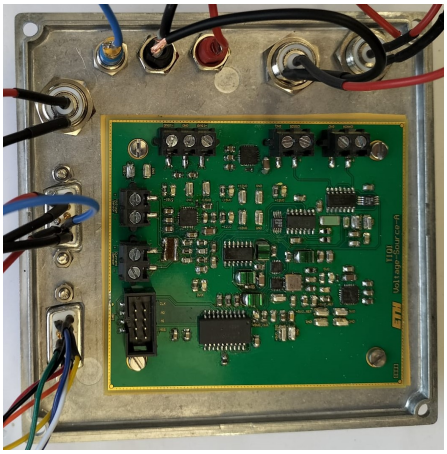

Figure 4: Inside view of the lid

The PCB is also susceptible to external electric fields, hence it has to be placed in an aluminium box acting as a Faraday cage. (See Figure 3 for top view, 4 for lid inside and 7 for side view).
The PCB is attached to the inside of the lid of the box. Over the cover, a block of aluminium 2 cm thick, with basis dimensions of 9.5x9.5 cm, is present. The box has basis dimensions of 12x12 cm. The aluminium block and the board are attached together via four screws going through the box lid at the corners of the PCB. A thermal pad is also placed between the cover and the board to help with uniformity of heat diffusion. This is necessary for metal-non metal interfaces and in compensating the roughness of the surfaces.
The temperature controller is connected to the aluminium block through the screw that gets heated up by the power dissipated by resistor 2R7 (see Figure 2). The screw will then diffuse heat inside the aluminium piece, which is connected to the PCB through the cover and the thermal pad. In this way, the temperature controller, while being placed outside to avoid the injection of electrical noise into the PCB, should act on the board to maintain its temperature constant.
All the connectors for the inputs and outputs of the PCB are also placed on the lid, next to the piece of aluminium. In particular, they are positioned as close as possible to the corresponding I/O of the board. The corresponding wires were also soldered to the connectors and hooked up to the PCB. For the output signal, monitor and sensed voltage, BNC connectors were chosen. For the supply inputs (+15V, 0V, -15V) banana connectors were chosen. Finally, for SPI communication and sensed current D-SUB 9-pin connectors were used. This last choice for the sensed current was forced by the application. Indeed, in the case of study, the current flowing in the Helmholtz coils is measured using a LEM 200 ULTRASTAB, which works through a cable compatible with the D-SUB 9-pin. Out of the nine pins, only five were used: two for the actual sensed current and three for the supply of the LEM. Indeed, the three corresponding wires have to be soldered to the banana connectors that take in the cables from the board power supply. All the connectors are labeled directly on the casing.
The connectors and the PCB were placed below the lid for convenience, such that if there is a problem and the PCB has to be checked, this can be simply done by lifting the cover.
Finally, in order to prevent the generation of air fluxes inside the box, which could cause temperature fluctuations, a cloth of a non conductive material was inserted.

3 Software

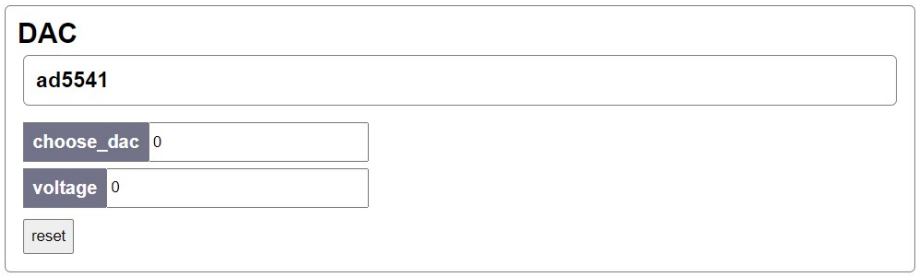

Figure 5: Web interface of the tested code for controlling the two DACs

A new code has been written in order to control the two DACs. Previously, one had to modify the program on the raspberry pi anytime a new reference had to be set. Now the code can be run only once, and the DACs can then be controlled through a web interface (see Figure 5). The software makes use of the TIQI plugin and all required packages for its functioning have been downloaded on the raspberry. Information on how to install TIQI plugin module can be found here: https://gitlab.phys.ethz.ch/tiqi-projects/tiqi-plugin. Ad5541 is the DAC type. Under "choose_dac", which of the two DACs one wants to control can be chosen: 0 for the coarse DAC, while 1 for the fine. Under "voltage" the value of the chosen DAC (expressed in Volts) can be inserted. If the value is greater than the maximum possible (1.9898V) or less than $0V$, it will not be taken and nothing will change. The SPI communication has been made such that only one DAC at a time can be set. This is the reason why one has to select a DAC, set the voltage and then select the other one. Finally, a reset button is also available. If pressed, it will set both DACs to zero.

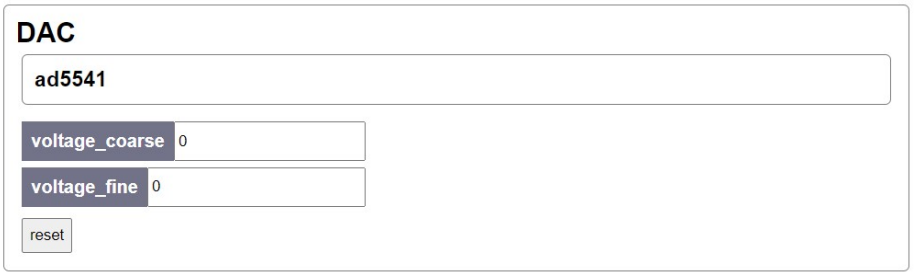

Figure 6: Newest version of the interface. Still under test

Another code, with a more intuitive interface (Figure 6), was then written, but not directly tested on the raspberry pi. With this, the user can directly set

both DACs with no need of changing selection, which is done in background.

The codes can be found at https://gitlab.phys.ethz.ch/tiqi-projects/drivers/tiqi-ad5541. AD5541.py is the driver used to implement the SPI communication. It differs from the one presented in [1] for not having the reset function, which has been added in the higher level code. The driver makes use of Spidev to work and so this should be downloaded on the raspberry. Moreover the driver should be placed in the same directory of the code to run. [1]
The code linked to the interface shown in Figure 5 is under the name main.py, while the code to be tested is main_to_test.py.

4 Characterization

4.1 Measurements and results

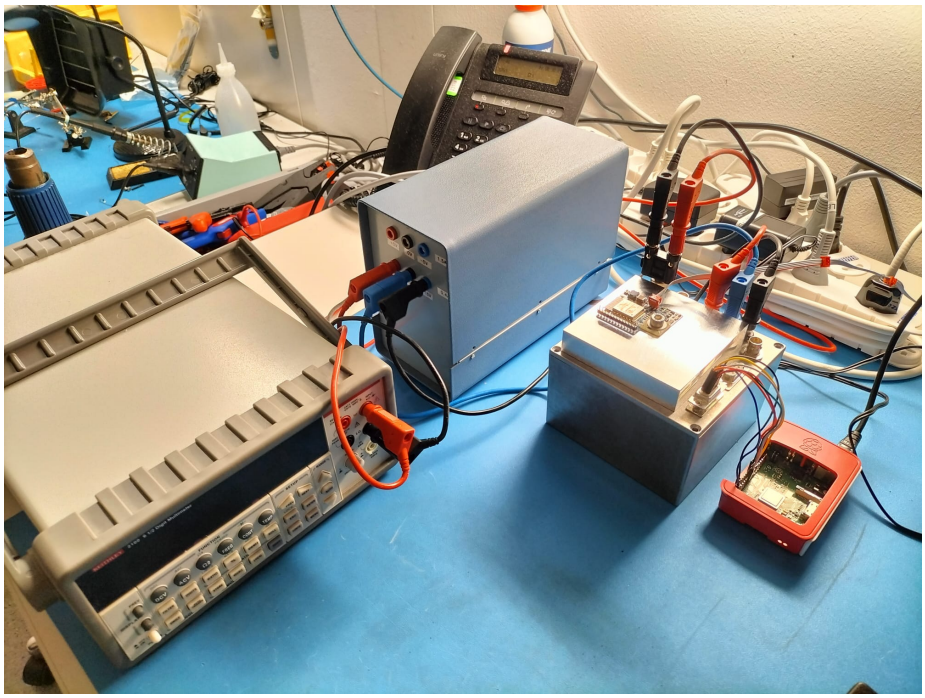

Figure 7: Measurement setup

After the realization of the device, characterization was performed. Some measurements had already been carried out in [1], hence the same DACs settings were chosen for better comparison. A new power supply was used though. However, given the presence of the voltage regulators, it should not have a great impact on the results.
As a first step, a measurement of the output signal with the sensed current and voltage inputs shorted and with $V_{DAC_{coarse}} = 0.02V, V_{DAC_{fine}} = 0.5V$ was performed in the office. The results are shown in Figure 8. In particular, the displayed data are taken starting from two hours after the system was turned on, in order to let the PCB and the temperature controller stabilize. The data points were taken roughly every 25ms from 11:30 to about 18:15 using a keithley 2100 6 1/2 digit multimeter.
Being white noise present, data are uncorrelated and so standard deviation is a good estimation of the uncertainty the output signal will be subject to. The results are characterized by a standard deviation in the order of $10^{-4}V$,

better than the $10^{-3}V$ of the data shown in Figure 4.4(b) in [1]. However, a direct comparison can not really be performed as the time span considered by the previous student is much larger and the period of the year is also very different. Hence, it is not certain whether the results are better thanks to the new casing or simply because temperature was more stable the day the new measurement was performed. Also, a slow drift towards smaller values is visible in the plot on Figure 8, which corresponds to the decrease in temperature the office room was subject to during those hours. This result then suggests that the temperature controller is not working as expected. This might be due to the fact that the set-point is chosen automatically and can require even days in order to be properly set. So the controller either hasn't reached this point or was not working at all.

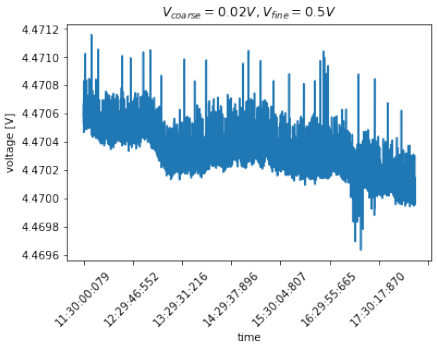

Figure 8: Plot of data obtained measuring in the office the output signal of the error generator

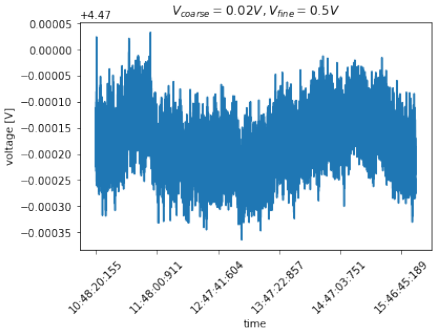

Figure 9: Plot of data obtained measuring in an AC controlled room the output signal of the error generator

In Figure 9 the results from a measurement with the same parameters than before, but performed in a room with air conditioning on, are shown. In particular, the displayed data cover a time period of five hours after a couple of hours for stabilization. A greater stability in temperature is reflected in a greater stability in the output signal, which is characterized by a standard deviation of $4.57 \cdot 10^{-5}V$.
Also from this results it is hard to extrapolate how the temperature controller is working. Hence, a new experiment was performed: The device was turned on and let to stabilize for a few hours. Then, variations in temperature were forced by using a heat gun from quite far, such that the box did not get too hot. The output signal was recorded and the plot showing the results is displayed in Figure 10. From these data it is clear that the PCB is still sensible to changes in temperature. Indeed, the two jumps at 17:30 and 17:45 corresponds exactly to the moments in which the heat gun was turned on.
Hence, the implementation of the temperature controller needs to be revisited. For example it could be manually set at a couple of degrees more than the expected maximum temperature of the room it will be placed in. Also, a more rigorous study of its behaviour could be performed by making use of the available

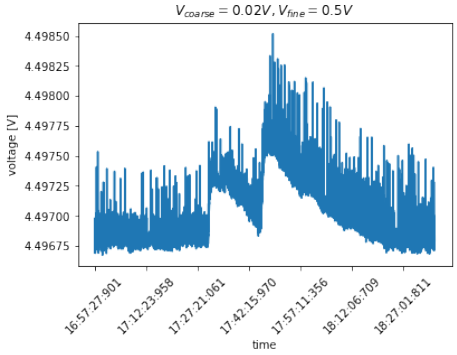

Figure 10: Plot of error voltage forcing temperature variations

Grafana option.
Other external sources of noise could be given by the power supply of the PCB and the multimeter itself. Their time trace was then also measured. In the case of the multimeter, its input was shorted. The results for the latter are characterized by a standard deviation of about $7 \cdot 10^{-7} V$, while data from the supply measurement show a standard deviation in the order of $10^{-4} V$. However, as pointed out before, the inputs from the supply go through the voltage regulators, which stabilize them. Simulation of their action are shown in [2]. Hence, these two elements are not dominant sources of noise.

Finally, a new set of measurements was performed with the help of Engineer Peter Maerki from the Ensslin group in order to probe the noise spectral density of the device. Previous measurements were carried on with the keithley 2100 6 1/2 digit multimeter whose maximum sampling speed is of 25ms per sample, which means that in principle only noise below 20Hz can be probed.
Sensed current and voltage inputs were left open. It was decided to not apply any current to not be sensible to noise coming from the current source. However, the device noise can depend on the current flowing through it, hence the results are an underestimation of the total noise. Moreover, they were left open and not shorted in order to see Johnson noise coming from the input resistors.
Figure 11 displays the results of some of the measurements that were performed. The orange trace shows the noise of the oscilloscope which was used. This is background noise due to the measurement itself and so it should be subtracted to all other results. The red trace represents the noise of the output signal with both DACs set at $0V$ and the whole setup present (PCB connected to raspberry pi which is connected to the PC via an ethernet cable). Below $1kHz$ some anomalous noise is present. The same measurement, which is not shown, was also performed with the output of the coarse DAC set at $1.9V$. The same results were obtained, hence the anomalous noise is dominating over the noise coming from the reference of the DAC. In order to find its source, the computer, which was sitting close to the PCB, was disconnected from the raspberry pi and placed far and the power supply of the Pi was changed from a switch mode to a linear mode one. Data obtained in this conditions are shown in black. It is clear that they resemble the previous ones. Hence, the raspberry was disconnected from the PCB. Results are shown in green. A much cleaner spectrum is obtained,

suggesting that the raspberry pi was the source of the anomalous noise. However, between the Pi and the DACs an isolator is placed (see Appendix A, U500), which should isolate the digital and analog signals and, in particular, their respective grounds. Due to a mistake in the design, this last thing does not happen. Signal VDD_3V3-5V0, which comes from the Pi, is connected to the analog ground through resistor R907 and LED D907. One of these two should then be unsoldered. Studying the design further, another design mistake was found. Operational Amplifier U300D, which is a spare part, has the inputs connected to ground through resistors R306 and R307. Hence, $V_+ - V_-$ should be set at $0V$, but fluctuations could occur and, given the very large gain of the OpAmp, they would be greatly amplified. So, resistor R306 should be unsoldered and V_- input should be shorted with the output in a negative feedback loop.

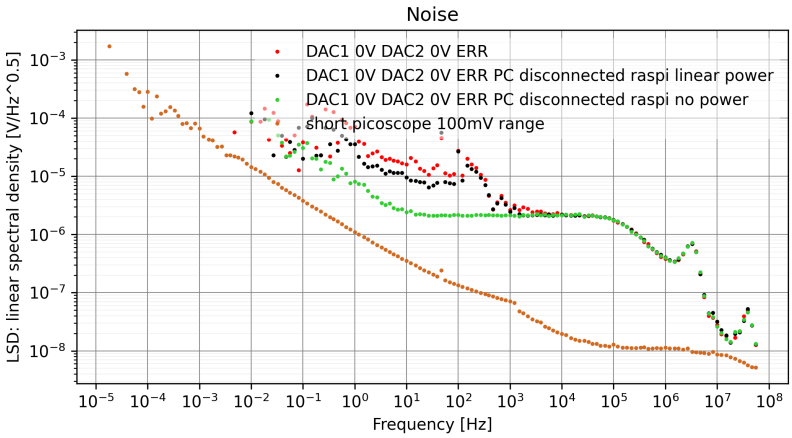

Figure 11: Plot of noise spectral density of the output signal for different measurement setup configurations

Coming back to Figure 11, the noise measured shows white noise at $2\frac{\mu V}{\sqrt{Hz}}$ and flicker noise equal to $17\mu Vrms$. The latter has been obtained by evaluating the integral of the power spectral density (expressed in $\frac{V^2}{Hz}$) between 0.1 and 10 Hz, which is the usual interval where flicker noise is evaluated. Finally, the reasons behind the shape of the spectral density after $10^5 Hz$ were not fully understood.

4.2 Comparison with system currently in use

Once the results were obtained, the system under study was compared to the one currently being used at TIQI. Unfortunately, data from the characterization of the latter were not directly available, hence a software for image analysis called

"imageJ" was used in order to retrieve some of them from the plot in Appendix C3 (Figure 16). In particular, only data from the reference voltage noise spectral density were considered as those from the sensor voltage are heavily influenced by LEM noise, which was not taken into account in the measurements shown in the previous section. As one can see in Appendix C1 (Figure 14), the resistors and capacitors at the final stage can be chosen by the user. The only way to get to know what's being used would be to open the box and directly look into it. However, this was not an option. A second identical error generator, which was used by Dr. Christa Fluhmann during the characterization process (see Figure 15), was checked. In this board, two $10k\Omega$ resistors are used, the capacitor in series with the resistor is not present, while the one in parallel has a capacitance of $10pF$. This capacitor introduces a pole at $16MHz$, comparable with the OpAmp pole, hence, in the frequency region of interest (below $10^5 Hz$) the output will be equal to $2V_{ref} - V_{sensed}$. As a consequence, the noise spectral density of the reference voltage has to be multiplied by two.

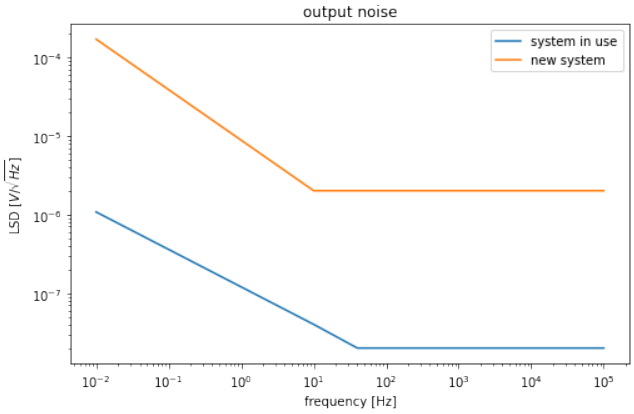

Figure 12: Plot of the interpolated noise estimation of the output of the error signal generator under study versus the one currently being used.

Data taken from [3] and those in green in Figure 11 were interpolated. Results are shown in Figure 12. The output noise of the device under study is two orders of magnitude higher than the one currently being used. It is mainly due to the fact that in the new system the reference is controlled digitally and that then there is a gain of 200. The two DACs have a white noise of $11.8nV/\sqrt{Hz}$, hence after the multiplication by 200, noise will already be in the microvolt order of magnitude. Furthermore, before the amplification stage there are four OpAmps (three from the DIFF_SIG part and one from the V_DAC_{coarse} part), which introduce noise too.
However, the output noise of the error generator is not the significant quantity to compare. In particular, we are interested in the noise of the current at Helmholtz coils level. So, the whole control system should be taken into account. The following calculations will show that, in principle, a noisier error signal generator can have better performances. Indeed one of the reasons why the system under study is noisier than the one currently being used in the TIQI setup is that it has a much higher gain. However, in the final noise there will be a division by

this gain.
An abstraction of the control system is given in Figure 13, where:

$$I(t) = I_0 + s(t) + u(t)$$
$$e(t) = \alpha(V_{ref} - V_{sensed}(t)) + n(t)$$
$$V_{sensed}(t) = \beta I_{sensed}(t)$$
$$I_{sensed}(t) = \gamma I(t) + \xi(t)$$

$I(t)$ is the current going to Helmholtz coils, I_0 is the desired current, $s(t)$ is the noise coming from the current source (Agilent 6682A), α is the error generator gain, $n(t)$ the output noise of error generator, β the gain for the current-voltage conversion inside the device and γ is the LEM gain. Finally, $u(t)$ is the control signal produced by the Agilent itself. However, from the manual, it is not clear what is the relation between $e(t)$ and $u(t)$. Then, for simplicity, $u(t) = k \cdot e(t)$ will be assumed. With this in hand, after some algebra, one can find:

$$I(t) = \frac{1}{1+k\alpha\beta\gamma}[I_0 + k\alpha V_{ref} + s(t) + kn(t) - k\alpha\beta\gamma\xi(t)]$$
$$\implies N_{tot}(t) = \frac{1}{1+k\alpha\beta\gamma}[s(t) + kn(t) - k\alpha\beta\gamma\xi(t)]$$

where N_{tot} is the current noise at Helmholtz coils.

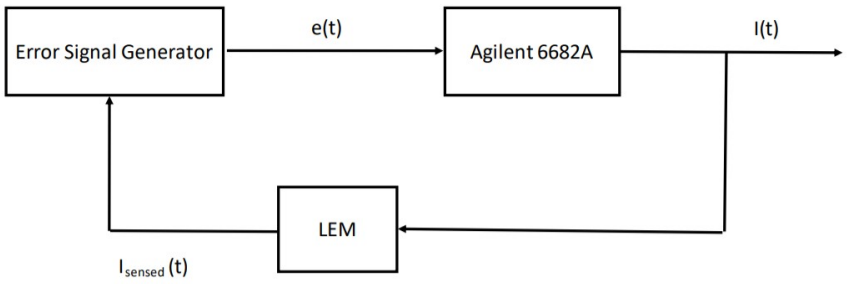

Figure 13: Block diagram of the control system

Known parameters for the two setups are:

$$\alpha_n = 200 \qquad \alpha_o = 1$$
$$\beta_n = 4.32V/A \qquad \beta_o = 50V/A$$
$$\gamma_n = \gamma_o = 1/1000$$

where subscript "n" stands for "new" and "o" for "old". Also, V_{ref} for the old setup is twice the reference voltage of [3], as well as, as stated before, $n(t)$ is twice the one shown in Figure 16.
In order to make a comparison based on the plots shown in Figure 12 the previous

relation of N_{tot} will be considered in the frequency domain. With the given numbers, one can get:

$$N_{tot_n}(\omega) < N_{tot_o}(\omega)$$

$$\iff \quad n_n(\omega) < \frac{2500+2160k}{2500+125k}\left(\frac{2035}{2500+2160k}s(\omega) + \frac{407}{500+432k}\xi(\omega) + n_o(\omega)\right)$$

The result depends on the control signal gain, the source noise and the measurement noise. In the following, in order to compare the two error generators directly, a perfect control action will be assumed, hence that the output noise of the current supply is completely suppressed, i.e. $k \to \infty$.
In this limit one gets:

$$n_n(\omega) < 17.28 n_o(\omega)^{1}$$

However, as one can get from the plot in Figure 12, $n_n(\omega)$ is bigger than $17.28 n_o(\omega)$ by about one order of magnitude $\forall\omega$.
This result suggests that the device that has been built in this project will not have better performances than the system currently in use and so the substitution should not be realized. However, in the context of a new control system this last result could change.

4.3 Possible improvements

One key advantage of the proposed system is that it can be controlled from the computer. However, as stated above, the noise produced by the coarse DAC is greatly amplified. This is the limiting factor of the system. Another source of noise is given by the high number of components in the DIFF_SIG path, as they all produce noise which is then amplified by 200. In contrast, in the error generator currently in use at TIQI, the sensed voltage is simply produced by making use of two resistors in parallel.
A new design where the generation of the reference is produced by making use of DACs (with higher output voltages range) and the rest is taken from the system shown in Figure 14, could integrate the advantages of the two systems.
The implementation of a different value of β could also then be considered. The higher it is the more $s(t)$ would be suppressed, without affecting too much $n(t)$, as the gain is realized at the input stage. The maximum value of β is limited by ξ which would be greatly amplified. Also, if the gain is implemented by making use of resistors, one has to consider the power which would be dissipated, bringing to an increment in temperature and so an increment of Johnson noise.

[1] $17.28 = (\alpha_n\beta_n\gamma_n)/(\alpha_o\beta_o\gamma_o)$

5 Conclusion

In conclusion, the realization and characterization of an error signal generator for either a voltage or a current source has been completed. In particular, the casing for an already existing PCB has been constructed with the inclusion of a temperature controller. Results obtained during the characterization process show that the implementation of the latter needs to be revisited. During this process, two mistakes in the PCB design were also found:
- Resistor 306 should be unsoldered and the inverting input of OpAmp U300D should be shorted with its output.
- Either R907 or D907 should be unsoldered.

The most significant result is the green plot in Figure 11. It shows the output noise of the error generator with no inputs given, besides the supply. Since there is no current flowing through the DIFF_SIG path and $0V$ output of the DACs, the obtained $17\mu Vrms$ flicker noise and the $2\mu V/\sqrt{Hz}$ white noise have to be taken as underestimations.
Originally, this device was thought to be used in the context of magnetic field stabilization for trapped ions systems, in order to increase the coherence time of qubits levels. However, it has been shown that the existing system for such a purpose has better performances. This result strongly depends on the specific control system considered and so it is not general. Moreover, magnetic field stabilization is also only a specific application of the device. In order to see whether this system could be useful, one should take the results presented in section 4.1 and include them in the calculations for their own control system. Finally, it has been noted that some sources of noise are due to the design itself and a new design with potentially improved performances has been suggested.

References

[1] Tenzan Araki, *Error Signal Generation for Ultrastable Voltage Source*, Semester Thesis ETHz (2021).

[2] Leon Raabe, *Ultra-Stable Error Signal Generator*, Semester Thesis ETHz (2020).

[3] Christa Fluhmann, *Encoding a qubit in the motion of a trapped ion using superpositions of displaced squeezed states*, PhD Thesis ETHz (2019).

A Schematics of the PCB

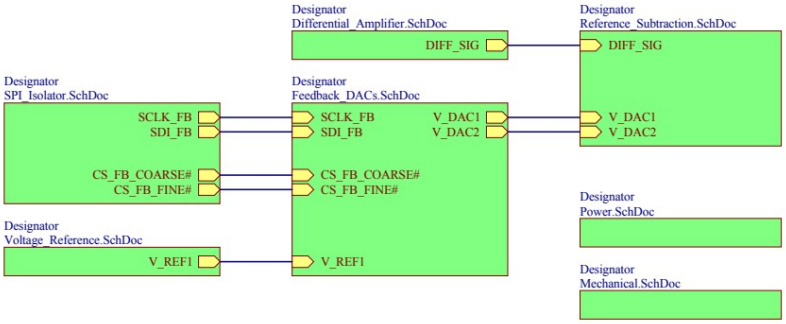

Differential Amplifier

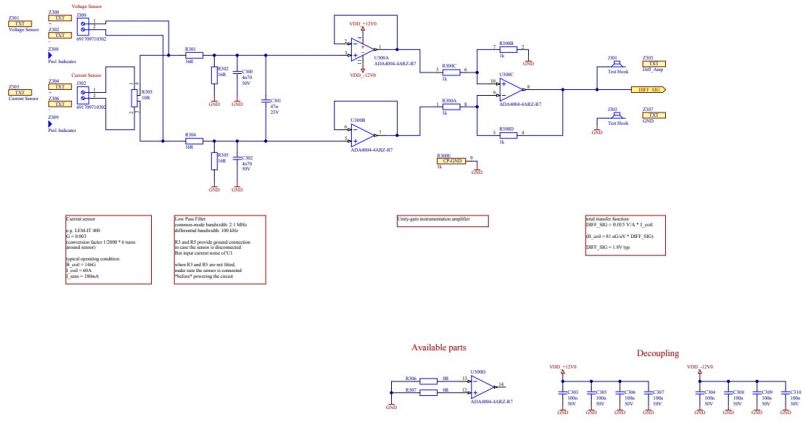

Reference Subtraction

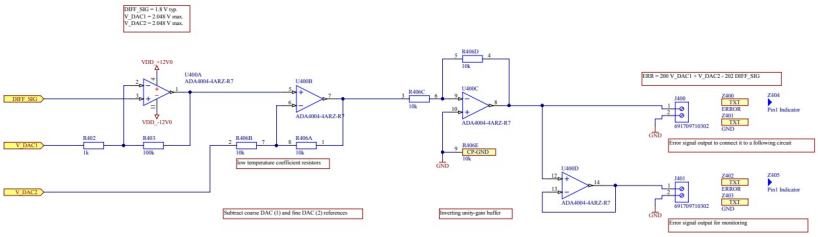

SPI Isolator

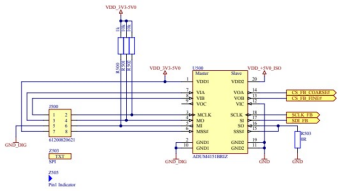

Decoupling

Voltage Reference

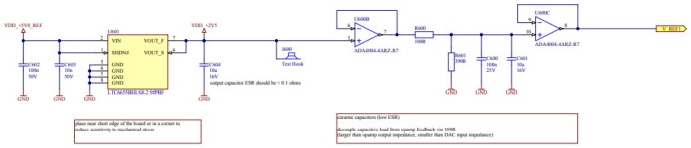

Feedback DACs

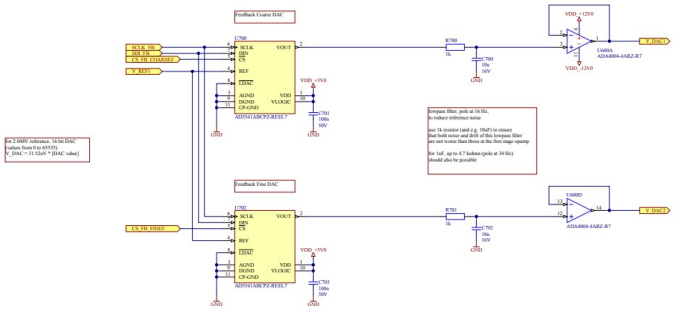

Decoupling

Voltage Regulators

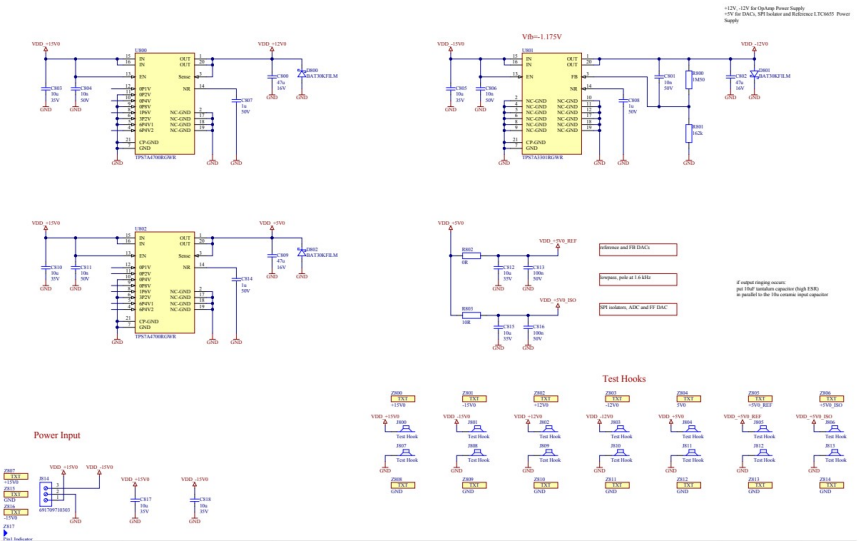

Mounting Holes

PCB / Fiducials

B Schematic of the temperature controller

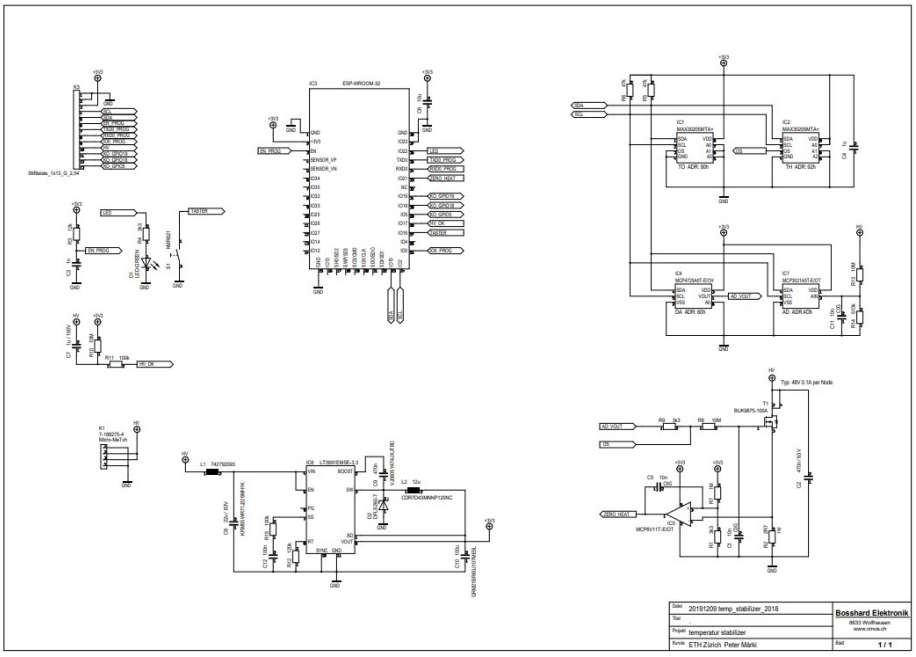

C Error generator currently in use at TIQI

C.1 Schematic of the board

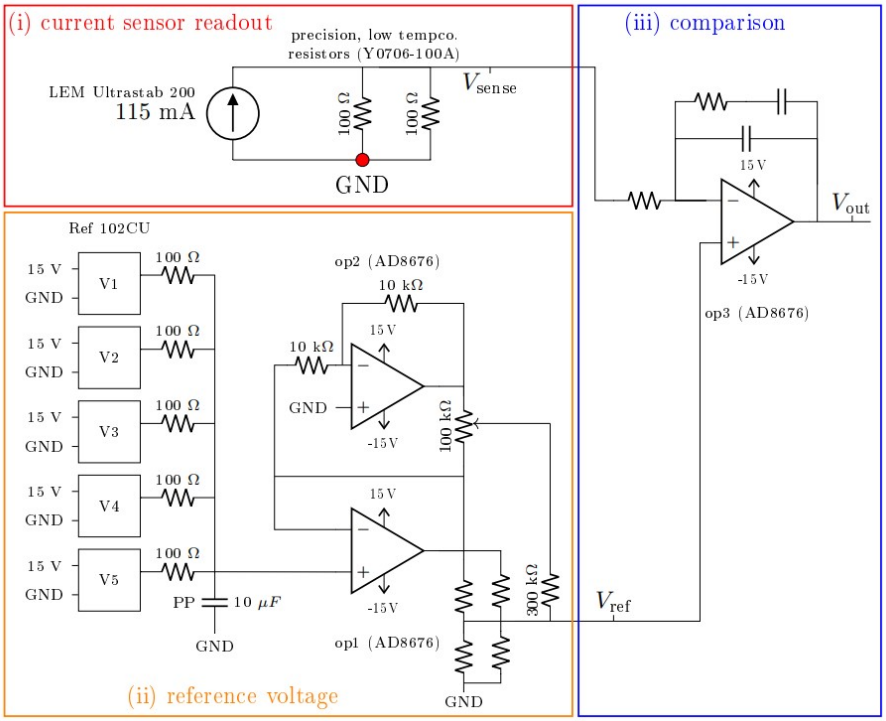

Figure 14: Error signal generator circuit. (i) Conversion of the fluxgate sensor (LEM Ultrastab 200) current to a readout voltage using two precision resistors. The sensor current is guided via thick wire (indicated by the red dot) directly to the PCB 0 V input. (ii) Production of a stable adjustable reference voltage using the averaged output of five 10 V low noise references. (iii) Comparison and feedback of sensor voltage V_{sense} to the reference voltage V_{ref}. Not shown are $1\mu F$ ceramic capacitors close to the power supply inputs of each OpAmp and the voltage reference. Further not shown is the input voltage filtering using 470 µF PET capacitors.[3]

C.2 Measurement setup

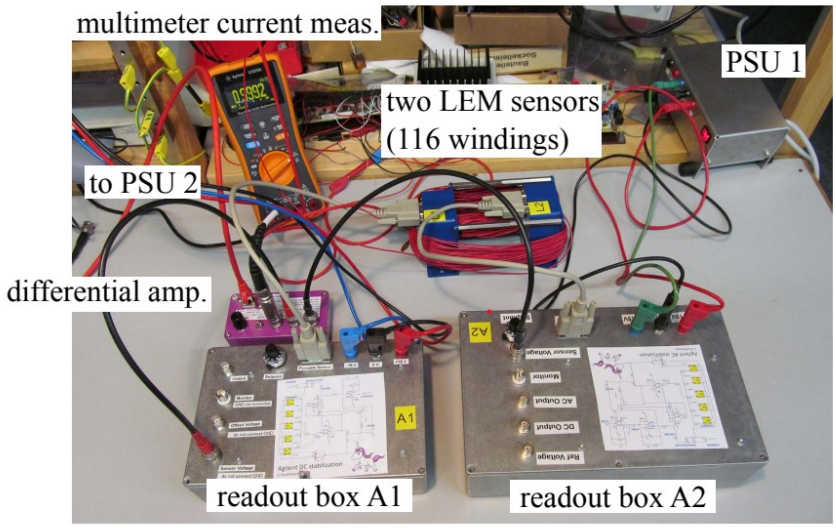

Figure 15: Setup used for the characterization of noise in the slow current stabilization. Not shown on the picture is the used current source as well as PSU2. LEM sensors denote the two fluxgate sensors.[3]

C.3 Measurement results

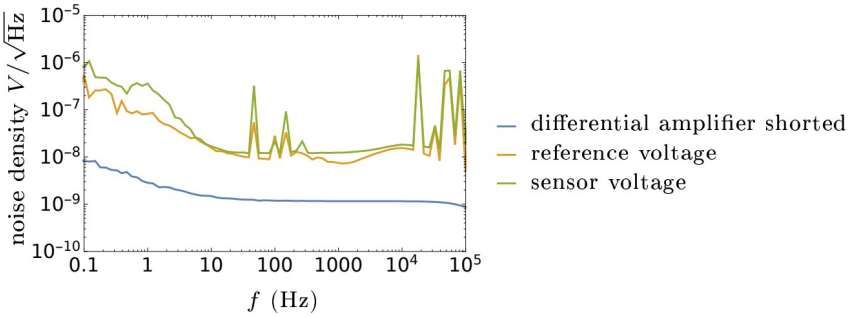

Figure 16: Noise analysis of the error signal generator. Using a low noise differential amplifier the fluctuations of two magnetic field stabilization systems are subtracted. The blue line shows the noise characteristic of the differential amplifier itself, which confirms a low background noise due to the measurement. Yellow shows fluctuations in the two reference voltages V_{ref} before they are compared by op3 (see Figure 14), green: fluctuations in the V_{sense} readouts of the 116 A current. Spikes at 50 Hz and multiples are due to the electronics in the vicinity of the test setup and do not reflect the situation in the experimental system. Spikes around $10^4 - 10^5$ Hz are due to the switching of the fluxgate sensor. These peaks should be filtered away by the integrating element of the feedback loop.[3]